BRDF Models for Accurate and Efficient Rendering of Glossy Surfaces

JOAKIM LÖW, JOEL KRONANDER, ANDERS YNNERMAN and JONAS UNGER
Linköping University

This paper presents two new parametric models of the *Bidirectional Reflectance Distribution Function* (BRDF), one inspired by the Rayleigh-Rice theory for light scattering from optically smooth surfaces, and one inspired by micro-facet theory. The models represent scattering from a wide range of glossy surface types with high accuracy. In particular, they enable representation of types of surface scattering which previous parametric models have had trouble modelling accurately. In a study of the scattering behaviour of measured reflectance data, we investigate what key properties are needed for a model to accurately represent scattering from glossy surfaces. We investigate different parametrizations and how well they match the behaviour of measured BRDFs. We also examine the scattering curves which are represented in parametric models by different distribution functions. Based on the insights gained from the study, the new models are designed to provide accurate fittings to the measured data. Importance sampling schemes are developed for the new models, enabling direct use in existing production pipelines. In the resulting renderings we show that the visual quality achieved by the models matches that of the measured data.

Categories and Subject Descriptors: I.3.7 [**Computer Graphics**]: Three-Dimensional Graphics and Realism; I.3.3 [**Computer Graphics**]: Picture/Image Generation

General Terms: Design, Performance

Additional Key Words and Phrases: BRDF, gloss, Rayleigh-Rice, global illumination, Monte Carlo, importance sampling

ACM Reference Format:

—

This work was funded through the Swedish Foundation for Strategic Research through the strategic research centre MOVIII grant A3:05:193, the Swedish Knowledge Foundation grant 2009/0091, Forskning och Framtid grant ITN 2009-00116, the Swedish Research Council through the Linnaeus Center for Control, Autonomy, and Decision-making in Complex Systems (CADICS), and the Excellence Center at Linköping and Lund in Information Technology (ELLIIT).

Authors' addresses: J. Löw, J. Kronander, A. Ynnerman and J. Unger, Linköping University, SE-60174 Norrköping, Sweden; email: {joakim.low, joel.kronander, anders.ynnerman, jonas.unger}@liu.se.

DOI 10.1145/XXXXXXX.YYYYYYY
http://doi.acm.org/10.1145/XXXXXXX.YYYYYYY

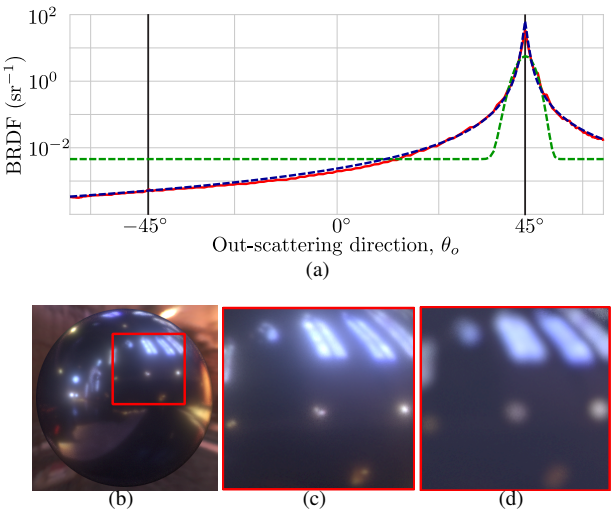

Fig. 1. A comparison between the new smooth surface BRDF model presented in this paper and the Cook-Torrance model. Figure (a) shows a log-scale plot of the scattering curve of a measured blue metallic paint (solid red), in the plane of reflection, for a light beam incident at 45° from the surface normal. The blue and green curves are the scattering curves of the proposed model and the Cook-Torrance model respectively. Figure (b) shows a sphere rendering using the measured BRDF data. (c) and (d) show close-ups of renderings using the new BRDF model and the Cook-Torrance model, respectively.

1. INTRODUCTION

Accurate modelling of light scattering at surfaces is a central component of photorealistic rendering in computer graphics. Reflectance modelling traditionally uses *parametric* models, empirically or physically based, of the *bidirectional reflectance distribution function* (BRDF) to represent scattering. Such models are often aimed at specific classes of surfaces, and in the case of physics-based models, are limited to surfaces fulfilling the underlying assumptions of the model. To enable reproduction of light scattering from arbitrary types of surfaces, modern research has put increasing focus on *data-driven* models [Lensch et al. 2005; Weyrich et al. 2008]. Data-driven models come with a cost, however, with less control and lower efficiency. Parametric models are lightweight and fully described by only a few parameters. The parameters often map intuitively onto the model behaviour, and efficient methods for off-line rendering are usually available.

In this paper, new parametric isotropic BRDF models are designed, based on the observations of the scattering behaviour of real glossy surfaces, extending the class of glossy surfaces which can be accurately represented by parametric modelling. The new models are inspired by scattering models from Rayleigh-Rice theory for

Table I. Notation

Symbol	
L	Incident light vector
L_P	Component of L parallel to surface tangent plane
R	Reflection vector
R_P	Component of R parallel to surface tangent plane
V	View vector
V_P	Component of V parallel to surface tangent plane
N	Surface normal
H	Unnormalized halfway vector: $L + V$
$\hat{H}$	Halfway vector: $H/\|H\|$
D_P	Projected deviation vector: $V_P - R_P$
$\omega_i = (\varphi_i, \theta_i)$	Spherical coordinates of L
$\omega_o = (\varphi_o, \theta_o)$	Spherical coordinates of V
$\omega_h = (\varphi_h, \theta_h)$	Spherical coordinates of $\hat{H}$
(r_i, ϕ_i)	Polar coordinates of L_P
(r_o, ϕ_o)	Polar coordinates of V_P
$\rho(\omega_i, \omega_o)$	Bidirectional reflectance distribution function
$r(\omega_i)$	Directional-hemispherical reflectance
$PSD(f_x, f_y)$	Power spectral density
$S(f)$	Condensed ABC model
A, B, C	Parameters of condensed ABC model
$F(\theta; \eta)$	Fresnel reflectance factor
G'	Smooth surface BRDF obliquity factor
Q'	Smooth surface BRDF polarization factor
$E_1(p), E_2(p)$	Error measures used for BRDF data fitting

optically smooth surfaces and micro-facet theory, adapted to accomodate for variations in reflectance behaviour observed in scattering data. The models closely reproduce the quality of the measured data when used in rendering, while maintaining editability through parameters with predictable behaviour, thereby enabling artistic fine-tuning.

To investigate the light scattering behaviour of different glossy surfaces, this paper conducts a study of measured BRDFs from the MERL database [Matusik et al. 2003]. The study focuses on properties with consequences for two key aspects of BRDF modelling, *parameterization* and *scatter distribution*. The first BRDF model presented is parametrized by the *projected deviation vector*, the deviation of the scattering (or view) direction from the mirror direction, projected onto the unit disk (Figure 2). This vector is closely connected to the parametrization of the Rayleigh-Rice BRDF model, and is shown to work well for the measured reflectance data in the study. Previous models in computer graphics have used constructs similar to the projected deviation vector [Neumann et al. 1999; Edwards et al. 2006]. In order to clarify the effect on parametric reflectance modelling, we investigate and compare the vector to the halfway vector for parametrization. To represent the scatter distribution of the BRDFs, which ranges from Gaussian-like to inverse-power-law-like, the ABC-model [Church et al. 1989] for surface statistics of optically smooth surfaces is utilized. The second BRDF model, based on the halfway vector, is constructed by assuming an ABC-model-like facet slope distribution in the Cook-Torrance BRDF model [Cook and Torrance 1982]. To enable efficient rendering, we also develop closed-form expressions for approximate importance sampling of the new models.

The main contributions in this paper can be summarized as:

(1) A study of measured reflectance data of glossy surfaces to identify components needed in parametric modelling, with a focus on parametrization and scatter distribution.

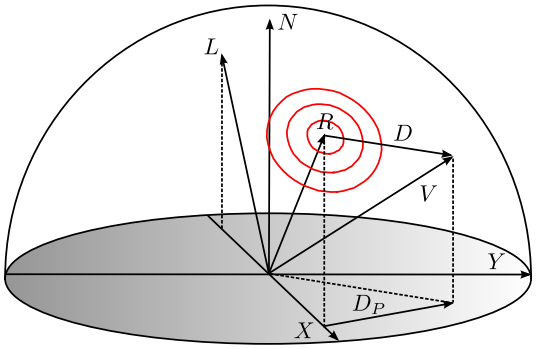

Fig. 2. The vectors involved in many BRDF models. The vector D_P, in this text referred to as the *projected deviation vector*, is the deviation, D, of the view direction, V, from the mirror direction, R, projected onto the unit disk. In the figure, contour lines of a Phong lobe are shown around the reflection vector. Contour lines on the hemisphere will be used later to show the shape of the gloss for various BRDFs.

(2) Two new parametric BRDF models, aimed at reproducing scattering behaviour observed in the study. One of the models is inspired by the Rayleigh-Rice theory for optically smooth surfaces, and the other is inspired by micro-facet theory. With modifications based on observations, the models enable accurate representation of light scattering properties of real world glossy surfaces.

(3) Derivation of closed form expressions for importance sampling of the new BRDF models to enable efficient image synthesis in a global illumination rendering framework.

2. PREVIOUS WORK

Reflectance modelling is a key part of the rendering pipeline, and the level of realism in a synthetic image depends on the accuracy of the models used. In physically based rendering, the BRDF is used to model surface reflectance. It is a real-valued function of four variables, $\rho(\varphi_o, \theta_o, \varphi_i, \theta_i) = \rho(\omega_o, \omega_i)$. It describes how light incident from the hemisphere around a surface point is scattered from the surface. In order for a BRDF to be *physically plausible* [Lewis 1993], it must obey *reciprocity*, i.e., $\rho(\omega_o, \omega_i) = \rho(\omega_i, \omega_o)$. It must also be *energy conserving*, which means the following relation must hold:

$$r(\omega_i) = \int_{\mathcal{H}^2} \rho(\omega_o, \omega_i) \cos\theta_o d\omega_o \leq 1, \quad \text{for all } \omega_i \in \mathcal{H}^2. \quad (1)$$

where r is the *directional-hemispherical reflectance* [Nicodemus et al. 1977]. The BRDFs studied in this text are *isotropic*. This means that the scattered intensity, in the azimuthal angle, is dependent only on the difference between the incident and outgoing (scattered) light directions:

$$\rho(\varphi_o, \theta_o, \varphi_i, \theta_i) = \rho(\varphi_o + \Delta\varphi, \theta_o, \varphi_i + \Delta\varphi, \theta_i), \quad \Delta\varphi \in \mathbf{R}. \quad (2)$$

Thus, for isotropic BRDFs, it is enough to study their behaviour for a fixed φ_i.

2.1 Computer Graphics

In computer graphics, there are several models of surface BRDFs available. Some of the most well-known empirical models are the Blinn-Phong [1977], Ward [1992], Ashikhmin-Shirley [2000], Lafortune [1997] and Neumann [1999] models. In addition to these

there are models inspired by real physical processes. They are derived from certain assumptions regarding the small scale (micro- or nano-scale) structure of the surface at hand. The Torrance-Sparrow [1967] and Cook-Torrance [1982] models are based on the assumption that the surface consists of a distribution of microfacets that reflect rays of light. This class of models is therefore often referred to as *microfacet* models. The model presented by He et al. [1991] is, instead, based on Kirchhoff diffraction theory.

Some work has examined the applicability of existing models. Ngan et al. [2005] make a comparison of several BRDF models by fitting them to a large database of measured materials, the Mitsubishi Electric Research Laboratories (MERL) database [Matusik et al. 2003]. Westin et al. [2004] also makes a comparison between BRDF models regarding their ability to model a smaller number of measured BRDFs, and reaches the conclusion that there is no single model that performs best at all times. To increase accuracy of fittings to measured data, multilobe versions of parametric models have been investigated [Lafortune et al. 1997; Ngan et al. 2005; Rump et al. 2008].

The BRDF is generally described as a function of four variables, a pair of spherical coordinates for each of the incident and outgoing directions. Alternative parametrizations can yield representations of fewer variables as well as cost-savings with regard to data-storage of measured data. Such parametrizations have been explored by Rusinkiewicz [1998], as well as Stark et al. [2005].

For efficient off-line rendering using Monte Carlo methods, it is beneficial to importance sample the BRDF model. Efficient importance sampling requires an analytical expression of a probability density function to draw samples from [Pharr and Humphreys 2010]. The probability density function should closely match the cosine-weighted BRDF, up to a normalization factor. Importance sampling schemes have been proposed for several previous models, using probability density functions either derived directly from the model distribution, or constructed to approximate it. Examples are the Blinn-Phong model [Pharr and Humphreys 2010], the Lafortune model [1997], the Ward model [Walter 2005], the Ashikhmin-Shirley model [2000], the model by Neumann et al. [1999] and the model proposed by Edwards et al. [2006]. For measured or complex analytical BRDF models, which do not lend themselves to closed form sample generation, factorization methods can be used for importance sampling [Lawrence et al. 2004].

Over the last decade data-driven BRDF modelling has grown more popular. In data-driven modelling, BRDF models use measured data in some form to represent surface reflectance. One of the most well-known databases of measured BRDFs is the MERL database [Matusik et al. 2003]. In addition to acquiring the reflectance data, Matusik et al. [2003] use the measured BRDFs as basis vectors of a larger space, building custom BRDFs as combinations of the measured BRDFs. Parametric BRDF models generally have an advantage over data-driven models by offering better control over the surface appearance through a few parameters. Therefore, effort has been put into finding factorizations of reflectance data that yield accurate yet intuitively editable data-driven BRDF representations [Lawrence et al. 2006].

2.2 Optical Engineering

BRDF models are commonly used in optical engineering to describe light scattering from rough surfaces, and to derive surface statistics from measured scatter data [Stover 1995]. Theoretical modelling and validation are active research areas. Different theoretical models are being employed and investigated, including the Rayleigh-Rice theory, Beckmann-Kirchhoff theory and the so-called generalized Harvey-Shack theory [Krywonos and Harvey 2006]. In our work, we draw inspiration from the Rayleigh-Rice theory for smooth surfaces, i.e., surfaces with structures small compared to the wavelength of visible light (see, e.g., [Stover 1995]):

$$\rho = \frac{16\pi^2}{\lambda^4} \cos\theta_i \cos\theta_o \, Q \, PSD(f_x, f_y). \tag{3}$$

PSD is the Power Spectral Density function of the surface, describing the surface statistics in terms of spatial frequencies, f_x and f_y. λ is the wavelength of the incident light, and Q is the reflectivity polarization factor, depending on the surface material properties. Expressions, and approximations for special cases, for this factor are given in [Stover 1995]. The two cosine factors together represent an obliquity factor, which causes a roll-off toward grazing angles. f_x and f_y are computed from the spherical coordinate angles of the incident and outgoing directions, θ_i, φ_o and θ_o, using the following relations:

$$f_x = \frac{1}{\lambda} \left(\sin\theta_o \cos\varphi_o - \sin\theta_i \right), \tag{4}$$

$$f_y = \frac{1}{\lambda} \sin\theta_o \sin\varphi_o. \tag{5}$$

It is important to note that these expressions have a close connection to the projected deviation vector, D_P, illustrated in Figure 2. Ignoring the division by λ, and assuming $\varphi_i = \pi$, f_x and f_y correspond directly to the two surface tangent space components of D_P.

Harvey [1977] observed the scattering behaviour of various reflecting surfaces in the reflection plane, i.e., the plane containing the incident and perfect reflection directions. When plotting the scattered radiance curves against $\sin\theta_o$ instead of θ_o, a *linear shift invariance* was discovered. This led to a linear systems formulation, which was later extended to the generalized Harvey-Shack theory. With a smooth surface approximation, this theory predicts a BRDF model very similar to the model resulting from Rayleigh-Rice theory [Harvey et al. 2007]:

$$\rho = \frac{4\pi^2}{\lambda^4} (\cos\theta_i + \cos\theta_o)^2 \, Q \, PSD(f_x, f_y). \tag{6}$$

Church et al. [1989] predicts the BRDF of optically smooth surfaces by measuring the surface profile of the surface finish, as a complement to direct BRDF measurement. They fit measured profile data to a surface power spectral density model called the *ABC* model:

$$PSD(f) = \frac{a'}{\left(1 + b^2 f^2\right)^{\frac{c+1}{2}}}, \tag{7}$$

where $f = \sqrt{f_x^2 + f_y^2}$, and

$$a' = \frac{1}{2\sqrt{\pi}} \frac{\Gamma((c+1)/2)}{\Gamma(c/2)} ab. \tag{8}$$

a is determined by low-frequency spectral density, $b = 2\pi l_0$ is related to the correlation length l_0, and $c > 0$ determines the fall-off of the spectrum at high frequencies. The ABC model is able to model the inverse-power-law shaped PSD of fractal surfaces, which Church and Takacs [1991] argue are the expected PSD shape of polished surfaces, and can be used, in addition, to model Gaussian-like PSD functions.

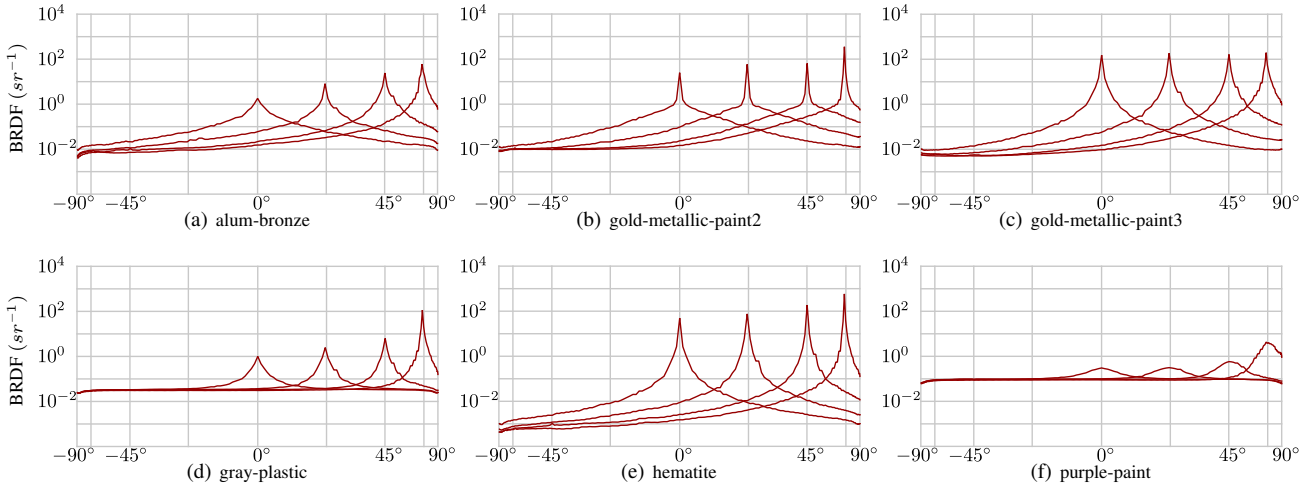

Fig. 3. Reflection plane plots of BRDF scattering curves in log-scale for incident angles $\theta_i = 0°, 22°, 45°, 67°$. The θ_o-axis is scaled by $\sin\theta_o$, revealing a symmetry around the reflection directions.

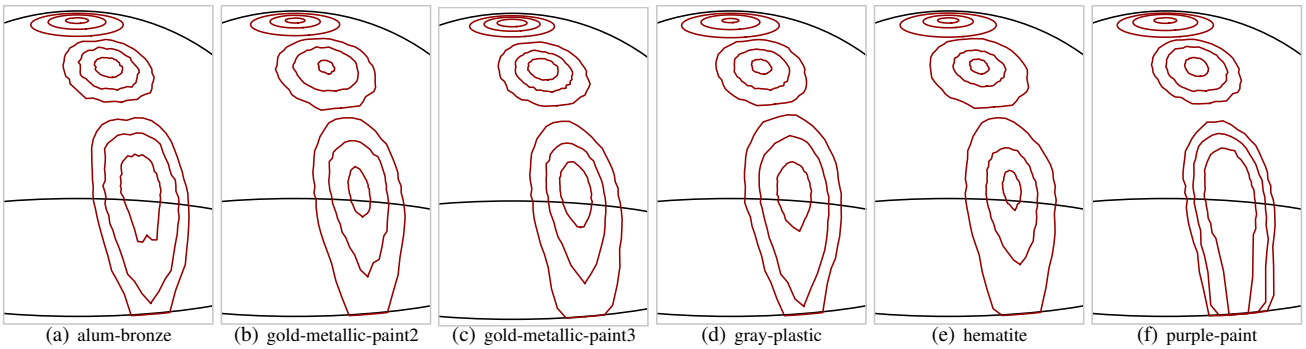

Fig. 4. Contour lines on the scattering hemisphere. Contour lines of the BRDFs are shown, for isovalues specified for each plot, for incident light at angles $\theta_i = 0°$, $25°$ and $60°$.

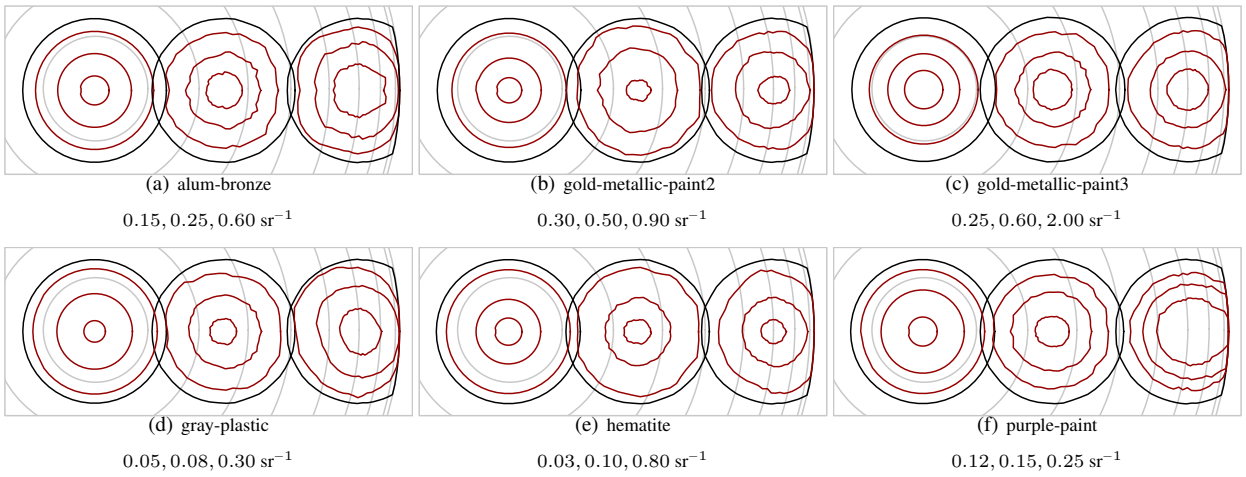

Fig. 5. Contour line plots in polar coordinates computed from spherical coordinates using $(r, \phi) = (\sin\theta, \varphi)$. Contour lines of the BRDFs are plotted, for isovalues specified per plot, for incident angles $\theta_i = 0°$, $25°$ and $60°$. Black circles are plotted to indicate constant distance from projected reflection direction, R_P, to help reveal the symmetry of the BRDFs. Gray lines correspond to azimuthal circles on the hemisphere, ten degrees apart.

3. BRDF MODELS FOR ACCURATE SCATTERING

This section presents a study which investigates the scattering behaviour of measured BRDFs. We are primarily interested in properties which affect the choice of *parametrization* and *scatter distribution* when designing new parametric BRDF models. The study also includes an examination of how different vector formulations affect the shape of the scattering lobe. The observations lead to two new parametric BRDF models, presented in Section 3.2.

3.1 Study of Measured BRDFs

A number of BRDFs from the MERL database [Matusik et al. 2003] are employed for a study: *alum-bronze*, *gold-metallic-paint2*, *gold-metallic-paint3*, *gray-plastic*, *hematite* and *purple-paint*. The chosen BRDFs exhibit glossy scattering behaviour, with significant wide-angle scattering, which is the focus of this article. Being isotropic BRDFs, they are studied using a fixed incident azimuthal angle, φ_i. For all plots in the study, the data from the red colour channel is used unless otherwise stated.

Measured Reflectance Data. In Figure 3, log-plots are shown of the BRDFs in the reflection plane, i.e., the plane containing the incident direction and mirror reflection direction. Note that the θ_o-axis is scaled by a factor $\sin\theta_o$ in the plots, although the corresponding angle, θ_o, is kept for reference at the reference lines. The scaling could be seen as an effect of projecting the BRDF sample locations on the hemisphere onto the unit disc.

It is apparent from the plots in Figure 3, that there is a symmetry around the reflection direction for all plotted incoming angles. Also, apart from a sideways shift, the shape of the wide-angle scattering is roughly invariant with respect to incident angle. This may be compared to the shift invariance property of scattering curves observed by Harvey [1977]. It is also consistent with Rayleigh-Rice theory, when isolating the effect of the PSD on the BRDF (Equation (3)). For scattering closer to the mirror direction, there is a steady increase in intensity as the incident angle approaches grazing angle, which is consistent with the well-known Fresnel effect.

In Figure 4, contour line plots on the hemisphere are shown for the BRDFs. In these plots, a spread of light towards grazing outgoing angles is observed for large angles of incident light. It is worth noticing that the scatter lobe does not get considerably narrower in the azimuthal direction, if at all, as the incident angle increases. This behaviour is also seen in Figure 5, where the contour lines of the BRDFs are shown in a polar coordinate system. In this figure, the radial coordinate is scaled by $\sin\theta_o$. This is emphasized in the plots by using reference lines corresponding to azimuthal circles on the hemisphere ten degrees apart. The BRDF contour lines have been chosen to show the shape of the surface gloss. As can be seen in the figure, the contour lines closely resemble circles. This means the symmetry observed in the reflection plane plots extends to circular symmetry around the specular direction. Furthermore, the off-specular linear shift invariance is valid outside the reflection plane as well.

From the scatter distributions in Figure 3 it is clear that none of the studied BRDFs, apart from the *purple-paint* BRDF, have shapes that resemble a Gaussian distribution. The peaks in the mirror direction are instead often sharp, and the scattering curves resemble an inverse-power-law curve. Wide-angle scattering is often approximated by a Lambertian component. On a logarithmic scale, it is apparent that only the *gray-plastic* and *purple-paint* BRDFs exhibit wide-angle scatter which could be accurately represented this way.

There is a small drop-off in intensity for several of the materials close to the grazing outgoing angles. However, the two metallic paints seem to be quite unaffected by attenuation effects. It should, however, be noted, as discussed by Ngan et al. [2005], that the measured BRDFs from the MERL database are unreliable for large incident and outgoing angles. Therefore, scattering curves for incoming directions near the grazing angle have also been excluded from the plots.

In summary, the most important observations of the studied BRDFs are:

(1) There is a symmetry of the scattering curves around the reflection direction, when projecting the sample positions from the hemisphere onto the unit disk.

(2) As the incident angle increases, off-specular parts of the scattering curves remain quite unaffected, apart from a sideways shift.

(3) The observed glossy scattering curves do not all resemble classical parametric distribution functions such as Gaussian or Phong-like functions. Instead, several BRDFs exhibit sharp scattering curve peaks, and large amounts of wide-angle scattering with an inverse-power-law shape.

Model Parametrization. The first two main observations above constitute requirements for a BRDF model to enable representation of real glossy surfaces. To find an efficient parametrization, three different vector formulations are studied to see if they fulfill these requirements; the deviation vector, $D = V - R$, the difference between the halfway vector and the normal, $\hat{H} - N$, and the projected deviation vector, $D_P = V_P - R_P$ (illustrated in Figure 2). The first two are chosen because of their relation to the Phong lobe, $\langle R, V\rangle^s$, and halfway vector lobe, $\langle N, \hat{H}\rangle^s$, respectively. The projected deviation vector, which is the deviation of V_P from R_P, i.e., the view and reflection vectors projected onto the surface tangent plane, can be efficiently computed using L and V accordingly:

$$H = L + V, \tag{9}$$

$$D_P = H - \langle H, N\rangle N, \tag{10}$$

where H denotes the *unnormalized* halfway vector. To compare the different vector parametrizations, a test lobe function is used: $\rho_T(f) = \max(1 - f^2, 0)$, where the length of the vectors are used as function arguments, i.e., $\rho_T(\|D\|)$, $\rho_T(\|\hat{H} - N\|)$ and $\rho_T(\|D_P\|)$. Figures 6 and 7 show contour line plots for the test function computed using the three different vectors.

Comparing the plots with the measured BRDFs in the study, one conclusion is that a model based on the deviation vector will not be able to properly model the symmetries observed in the plots of the measured BRDF data. The other formulations show a *relative* elongation in the θ-direction on the hemisphere near grazing incident angle. This can also be seen in Figure 8. The projected deviation vector, D_P, appears to be a good choice for model parametrization, since it preserves the circular symmetry around the reflection vector in the projected space (Figure 6) and is capable of preserving the spread of the gloss. At first glance the halfway vector parametrization seems to result in a lobe too narrow near grazing incident angles. Several previous models, however, have shown that the halfway vector can be successfully employed for BRDF modelling by introducing additional factors in the specular term to counteract this effect (e.g., [Cook and Torrance 1982; Ashikhmin and Shirley 2000]). Therefore both vector formulations will be used to construct BRDFs below.

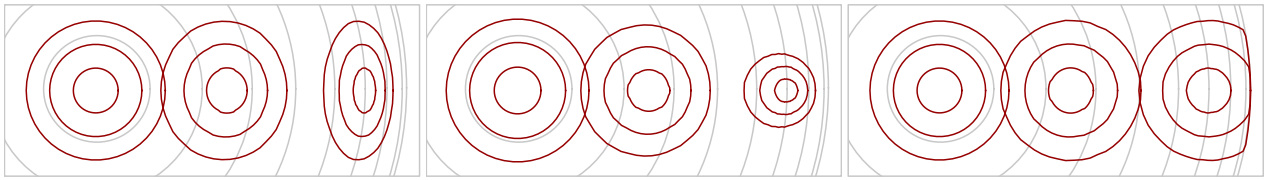

(a) $\rho_T(\|D\|)$ (b) $\rho_T(\|\hat{H} - N\|)$ (c) $\rho_T(\|D_P\|)$

Fig. 6. Contour lines of the test function ρ_T parametrized using the (a) deviation vector, (b) halfway vector and (c) projected deviation vector, plotted in a polar coordinate system using $\sin\theta_o$-scaling in the θ_o-direction. The halfway vector and projected deviation vector lobes preserve the circular shape around the projected reflection direction observed in the plots of the measured BRDFs, but only the last preserves the radius of the contour lines.

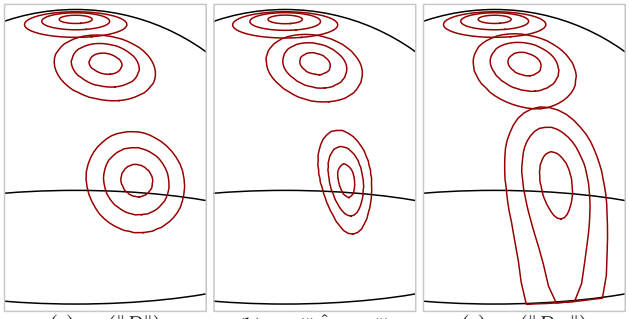

(a) $\rho_T(\|D\|)$ (b) $\rho_T(\|\hat{H} - N\|)$ (c) $\rho_T(\|D_P\|)$

Fig. 7. Hemispherical contour plots of the test function ρ_T parametrized using the (a) deviation vector, (b) halfway vector and (c) projected deviation vector, with contour lines chosen to show the relative change as the incident angle increases. Contour lines are shown for incident angles $\theta = 0°$, $25°$ and $60°$.

3.2 New BRDF Models

To model the scatter distribution shape of the studied BRDFs, and meet the third main observation from the study, the ABC model in Equation (7) will be employed in a slightly condensed version:

$$S(f) = \frac{A}{(1 + Bf^2)^C}, \tag{11}$$

where $A = a'$, $B = b^2$ and $C = (c+1)/2$. The shape of the model is shown in Figure 9 for varying B and C. Changing the parameters affects the shape of the model in a predictable way, with higher B producing more narrow specular peaks and C determining the fall-off rate of wide-angle scattering.

The BRDFs presented below are designed based on the observations in the study. They have not been modelled explicitly for energy conservation, but obey the reciprocity requirement of a physically plausible BRDF. As will be shown in Section 4, they also lend themselves to efficient importance sampling.

Smooth Surface BRDF. The observations made in the previous section indicate that the projected deviation vector is a natural choice for reflectance modelling. The new BRDF model is built by modifying the model in Equation (3). It uses the ABC-function to model the PSD, and does not take the wavelength into account. In addition to this, the model is relaxed by adding a Lambertian diffuse term, with scaling factor K_d, and allowing for a different obliquity factor, G':

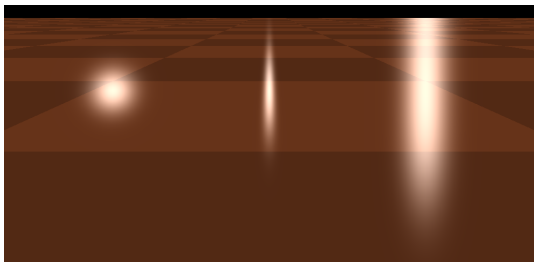

Fig. 8. Grazing angle reflections of the test lobe function raised to a power, ρ_T^s, to produce a narrow lobe, using the three different vector parametrizations discussed in the text.

$$\boxed{\rho = \frac{K_d}{\pi} + G'\, Q'\, S(\|D_P\|).} \tag{12}$$

There is no leading scaling constant for the specular term since scaling is taken care of by the A-parameter in S. Also, since only the square of the argument is used in the function expression of S, the square root involved in computing the length of D_P is avoided.

Two options for the obliquity factor, G', are implied in Equations (3) and (6). Because of unreliable data near grazing angles, however, we have chosen to let $G' = 1$ for the examples below. This choice is also in agreement with observations in Figure 3(b) and 3(c). The Q'-factor takes effects due to surface material properties, as opposed to geometry or structure, into account. For the experiments below, the Fresnel reflectance factor proposed by Cook and Torrance [1982], with extinction coefficient set to zero, is used as an approximation: $Q' = F(\theta_d; \eta)$.

The argument, θ_d, to the Fresnel factor is computed in the same way as in [Neumann et al. 1999]:

$$\theta_d = \arcsin\left(\frac{\|L_P - V_P\|}{2}\right), \tag{13}$$

where L_P and V_P are the surface tangent plane parallel components of L and V respectively. Computing the Fresnel factor involves the cosine of θ_d, which reduces to

$$\cos\theta_d = \sqrt{1.0 - \frac{\|L_P - V_P\|^2}{4}}. \tag{14}$$

Considering that the shape of the scattering curve for some measured BRDFs stays roughly constant for varying incident light angles, $Q' = 1$ could also be used as an approximation for some cases.

Although not used here, the Fresnel factor can be efficiently approximated according to Schlick [1994]. Note also that we are care-

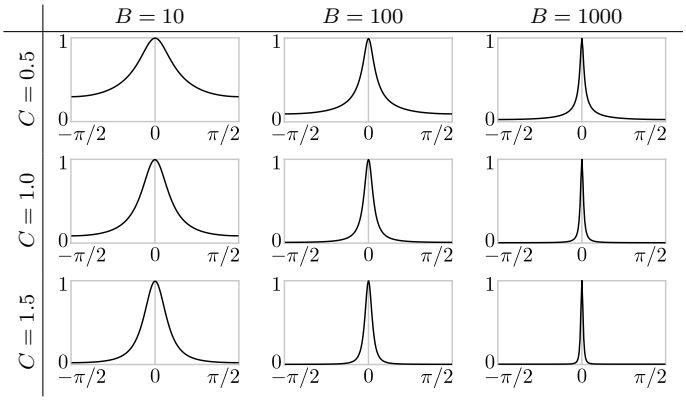

Fig. 9. ABC model curve for $A = 1$ and varying B and C. For the fitted BRDFs examined in this paper the values of C used in the plots above are common. For the parameter B however, a few BRDFs have a value as high as 10^6, which produces a very sharp and mirror-like reflection. In the plot the values are kept lower in order to yield a good understanding of the ABC model behaviour.

ful not to call η, the Fresnel reflectance parameter, 'index of refraction', since the Fresnel factor used is an approximation, and the parameter further loses it's meaning as index of refraction when used as a fitting parameter.

Microfacet BRDF. To create a model parametrized by the halfway vector, the Cook-Torrance model [1982] is modified to use an ABC-like distribution of micro-facets:

$$\boxed{\rho = \frac{K_d}{\pi} + \frac{S(\sqrt{1 - \langle \hat{H}, N \rangle})\, F(\theta_h; \eta)\, G}{\langle L, N \rangle \langle V, N \rangle},} \tag{15}$$

where G and F are the geometrical attenuation and Fresnel factors respectively, as described in [Cook and Torrance 1982]. θ_h is the angle between the normal and the halfway vector. The parameters are the diffuse parameter, K_d, the Fresnel parameter, η, and the A, B and C parameters of S. The A-parameter, as with the smooth surface model, is used for scaling the specular term which means that the S-factor does not directly represent a normalized facet-distribution.

Passing $\sqrt{1 - \langle \hat{H}, N \rangle}$ as argument to the ABC model function, S, has advantages for deriving closed form expressions for importance sampling, which will be discussed in Section 4. The square root never has to be computed explicitly, since S uses only the square of the argument.

4. IMPORTANCE SAMPLING

Efficient sampling schemes and variance reduction techniques are integral components in modern image synthesis where *Monte Carlo* methods for estimating light transport are used. The most fundamental method for reducing the variance of the estimators is *importance sampling*. The integral that must be evaluated is

$$L_o(\omega_o) = \int_{\mathcal{H}^2} L_i(\omega_i) \rho(\omega_o, \omega_i) \cos\theta_i \, d\omega_i, \tag{16}$$

where L_o and L_i are outgoing and incident light respectively. Using importance sampling, samples are drawn from a probability density where incident light directions, ω_i, are generated given a view direction, ω_o. For efficient sampling, the probability density function

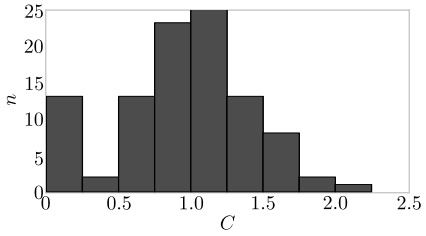

Fig. 10. A histogram over the C-parameter for all MERL BRDFs when fitted by the new smooth surface BRDF model.

should closely match the cosine weighted BRDF, $\rho(\omega_o, \omega_i) \cos\theta_i$, up to a normalization factor.

For importance sampling the new BRDF models, the inversion method [Pharr and Humphreys 2010] is used. To apply this method, a normalized probability density function must be found which has an invertible *cumulative distribution function* (CDF). To obtain tractable expressions for the new BRDFs, probability density functions matching the ABC-function alone are used. This is a common approach for importance sampling BRDF models since the distribution function often accounts for the largest variation in the BRDF model [Pharr and Humphreys 2010]. The effects of the other factors in the BRDF models are neglected, which means they can be changed without affecting the importance sampling schemes.

Smooth Surface BRDF. To find a density function, P_{ω_i}, on the hemisphere for the smooth surface BRDF we first consider a density function on the unit disk, P_d. The change from an area measure on the disk to a solid angle measure on the hemisphere requires a multiplication of $\cos\theta_i$, which means the cosine-weighting of the BRDF will be conveniently incorporated:

$$P_{\omega_i}(\varphi_i, \theta_i) = P_d(r_i, \phi_i) \cos(\theta_i), \tag{17}$$

with $(r_i, \phi_i) = (\sin\theta_i, \varphi_i)$. The density function, as well as the expressions for drawing random samples, are derived in polar coordinates. (r_o, ϕ_o) are the polar coordinates of V_P, the component of the view direction parallel to the surface tangent plane, and (r_i, ϕ_i) are the polar coordinates of L_P, the corresponding component of the incident direction to be generated. Expressing D_P in polar coordinates, we get:

$$\begin{aligned} \|D_P\|^2 = \|V_P - R_P\|^2 = \|V_P + L_P\|^2 = \\ = r_i^2 + 2 r_i r_o \cos(\phi_i - \phi_o) + r_o^2. \end{aligned}$$

To importance sample the smooth surface BRDF model, an approximation of the BRDF is used, setting $C = 1$. This provides a reasonable approximation for most real BRDFs (see Figure 10). Thus, the normalized probability density function, using the standard area measure on the disk, is

$$P_d(r_i, \phi_i) = \frac{M_d A}{(1 + B(r_i^2 + 2 r_i r_o \cos(\phi_i - \phi_o) + r_o^2))}. \tag{18}$$

M_d is the normalization factor

$$\begin{aligned} M_d = \frac{B}{\pi A} \Bigg[-\ln 2 + \ln \Bigg(1 + B - B r_o^2 \\ + \sqrt{1 + 2B(1 + r_o^2) + B^2 (1 - r_o^2)^2} \Bigg) \Bigg]^{-1}. \end{aligned} \tag{19}$$

Using the inversion method, expressions are found to draw samples distributed according to $P_d(r_i, \phi_i)$. Given two uniformly distributed random variables $\xi_1 \in [0, 1]$ and $\xi_2 \in [0, 1]$, samples are

generated by

$$r_i = \sqrt{\frac{(E-2)\,(E+2Br_o^2)}{2EB}}, \tag{20}$$

$$\phi_i = 2\arctan\left(\tan(\xi_2\pi)\sqrt{\frac{1+B(r_i+r_o)^2}{1+B(r_i-r_o)^2}}\right)+\phi_o, \tag{21}$$

where

$$E = \exp\left(\frac{\xi_1 B}{\pi A M_d} + \ln 2\right). \tag{22}$$

The corresponding probability density for the hemisphere, using solid angle measure, needed to weight the sample is then given by Equation (17).

Microfacet BRDF. For the microfacet BRDF model, recognizing that $\langle \hat{H}, N\rangle = \cos\theta_h$, a probability density function in half-angle space can be found as

$$P_{\omega_h}(\varphi_h,\theta_h) = \frac{M_h A}{(1+B(1-\cos\theta_h))^C}, \tag{23}$$

matching the facet distribution up to a normalization constant,

$$M_h = \begin{cases} \frac{B}{2\pi A \ln(1+B)}, & C=1 \\ \frac{B(C-1)}{2\pi A(1-(1+B)^{1-C})}, & C\neq 1 \end{cases}. \tag{24}$$

Given two uniformly distributed random variables, $\xi_1 \in [0,1]$ and $\xi_2 \in [0,1]$, a half-angle space direction, ω_h, is generated using

$$\theta_h = \begin{cases} \arccos\left(\frac{1+B-\exp[\xi_1\ln(1+B)]}{B}\right), & C=1 \\ \arccos\left(\frac{1+B-\left[1+\xi_1((1+B)^{1-C}-1)\right]^{-\frac{1}{C-1}}}{B}\right), & C\neq 1 \end{cases} \tag{25}$$

$$\varphi_h = 2\pi\xi_2. \tag{26}$$

Given a randomly selected halfway vector, $\hat{H}$ (corresponding to ω_h), an incident light vector, L (corresponding to ω_i), is computed using

$$L = -V + 2\langle V, \hat{H}\rangle \hat{H}, \tag{27}$$

where V is the given view direction.

The transformation from half-angle space to the sphere of incident directions yields a probability density for the generated incident light vector, as shown by for example Walter [2005]:

$$P_{\omega_i}(\varphi_i,\theta_i) = \frac{P_{\omega_h}(\varphi_h,\theta_h)}{4\langle L, \hat{H}\rangle}. \tag{28}$$

Generated half-angle space directions may produce incident directions on the hemisphere opposite to the surface normal. For these directions the integrand in Equation (16) is assumed to be zero-valued.

Generating samples two different expressions are obtained for the cases $C = 1$ and $C \neq 1$. In practice, numerical inaccuracies arise when drawing samples using Equation (25) for the case $C \neq 1, C \approx 1$, i.e., C is very close to one. For these cases, samples are drawn according to the case $C = 1$, this being a reasonable approximation to the real BRDF.

5. RESULTS

To evaluate the new BRDF models, they have been fitted to BRDF data from the MERL database, and rendered on spheres. The Cook-Torrance [Cook and Torrance 1982] and Ashikhmin-Shirley [Ashikhmin and Shirley 2000] models, with a Lambertian diffuse term, have been chosen for comparison.

5.1 Data Fitting

To fit parametric BRDF models to measured data, two different error metrics are used. The measured data, $\hat{\rho}$, and model values, ρ, are modified according to either

$$g_1(\omega_o,\omega_i;p) = \cos\theta_i \rho(\omega_i,\omega_o;p), \tag{29}$$

$$\hat{g}_1(\omega_o,\omega_i) = \cos\theta_i \hat{\rho}(\omega_i,\omega_o), \tag{30}$$

or

$$g_2(\omega_o,\omega_i;p) = \ln(1+\cos\theta_i \rho(\omega_i,\omega_o;p)), \tag{31}$$

$$\hat{g}_2(\omega_o,\omega_i) = \ln(1+\cos\theta_i \hat{\rho}(\omega_i,\omega_o)), \tag{32}$$

where p is the set of given parameters. For the logarithmic functions, the data values are incremented by one to avoid arbitrarily large negative values. The fitting is then performed in the least squares sense in MATLAB, using the *lsqcurvefit* command with a trust-region algorithm from the Optimization Toolbox:

$$\begin{aligned} E_m(p) &= \int_0^{\frac{4\pi}{9}}\int_0^{\frac{4\pi}{9}}\int_0^{2\pi} \left(g_m(\omega_o,\omega_i;p) - \hat{g}_m(\omega_o,\omega_i)\right)^2 \sin\theta_o\, d\phi_o\, d\theta_o\, d\theta_i \\ &\approx \sum_j\sum_k\sum_l \left(g_m^{jkl}(p) - \hat{g}_m^{jkl}\right)^2 \sin\theta_o^k \Delta\phi_o^l \Delta\theta_o^k \Delta\theta_i^j, \end{aligned} \tag{33}$$

with $m = 1$ or $m = 2$ given the choice of metric. The near-grazing angles are excluded since the measured data is unreliable for these angles [Ngan et al. 2005].

When the fitting is performed to the three colour channels simultaneously, the same set of parameters, except the diffuse and specular scale parameters, are used for all channels. The total error is computed as the sum of the above error for each channel. Since the measured reflectance data is isotropic, there is no need to integrate over φ_i, reducing the amount of computation needed. φ_o and θ_o are each sampled in one degree steps, yielding 360×80 samples per sampled incident angle, θ_i. Observing that the shape of the gloss changes slowly as the incident angle changes, the data is sampled sparsely over θ_i, with 10 degree steps. Ngan et al. [2005] suggest using a fast separable least squares approach for the fitting, but since one of the error functions, g_2, is non-linear in the parameters, this approach has not been used. The fitting computation is not time critical however, and only needs to be performed once.

The choice of error metric is not obvious, as the discussions and different choices of metric in [Ngan et al. 2005; Lafortune et al. 1997] show. The E_1 metric emphasizes the error in the specular direction, where the BRDF often has values several orders of magnitude larger than in its wide-angle scattering directions. However, larger weights may be desired for the wide-angle scattering, which is accomplished with the logarithmic error metric, E_2. We have found the results of the E_2 fitting metric to yield better visual reproduction of wide-angle scattering than E_1 for the new models presented in this paper, as can be seen in Figure 11.

Fittings to measured data for the new microfacet model and the original Cook-Torrance model are shown in Figure 12. Using the

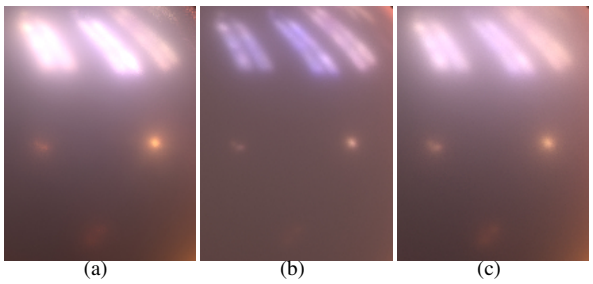

(a) (b) (c)

Fig. 11. Closeups from sphere renderings of the *alum-bronze* BRDF. (a) shows a rendering using the original measured data, while (b) and (c) show the smooth surface model using the E_1 and E_2 error metrics respectively for fitting to the measured BRDF.

logarithmic E_2 error metric forces the Cook-Torrance model to capture more of the wide-angle scattering than when using the E_1 metric. The latter produces better fitting to the specular peak, but excludes almost all wide-angle scattering. The effect of this is shown in Figure 13. It shows the results when rendering with the Cook-Torrance model fitted to measured data using the two different error metrics in 13(b) and 13(c) compared to the original data in 13(a) and the new microfacet model in 13(d).

Some materials have a distinct two-lobe shape, as shown in Figure 3(b). To handle these cases, we have investigated a two-lobe version of the smooth surface model, to increase fitting accuracy. In the plot, the wide-angle scattering stays roughly constant as the incident angle changes, while the small-angle scattering grows with increasing incident angle. Thus, only the second lobe uses a Fresnel factor, to account for the increase in intensity:

$$\rho = K_d + S_1(\|D_P\|) + F(\theta_d;\eta)\, S_2(\|D_P\|). \qquad (34)$$

Figures 17 and 18 show the curves of the new models fitted to the original data of three measured BRDFs. These plots show that the new models, when fitted to some measured BRDFs, are nearly indistinguishable from the original data. Figure 18(c) shows that the Fresnel approximation used fails in some cases for large scattering angles. This problem could be counteracted by using an attenuation factor, but should ultimately be corrected by using a more accurate Fresnel approximation.

In Table II the fitting errors are shown for the six measured BRDFs from the study. In the E_2 metric, the two new models generally have a smaller fitting error than Cook-Torrance and Ashikhmin-Shirley. For the *purple-paint* BRDF, the latter two models compete better with the smooth surface model, but the new microfacet model performs considerably better. Using the E_1 metric, the results are less one-sided, with the fittings of the smooth surface BRDF to *hematite* and the microfacet model to *gold-metallic-paint2* becoming worse than the models used for comparison. This indicates a worse fitting to the specular direction for the new models. All fitting errors should be put in perspective, however, by comparison with the resulting renderings, which shows the difficulty of drawing conclusions from the error metrics alone. This is further emphasized in the supplementary material to this text.

5.2 Rendering

The new BRDF models have been fitted to the BRDFs in the MERL database chosen for the study. For comparison of rendering quality, a number of spheres have been rendered using original measured data, Cook-Torrance, Ashikhmin-Shirley and the new models presented in this article. These are shown in Figure 16. For a fair comparison, we show renderings of the Cook-Torrance and Ashikhmin-Shirley models fitted to data using both of the presented error metrics, E_1 and E_2.

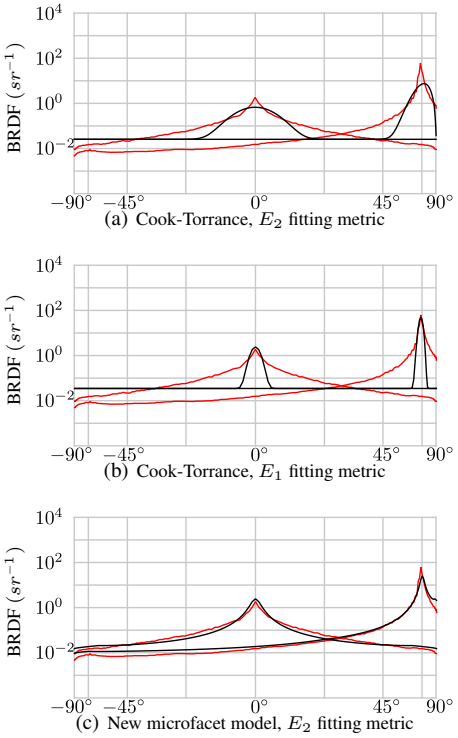

(a) Cook-Torrance, E_2 fitting metric

(b) Cook-Torrance, E_1 fitting metric

(c) New microfacet model, E_2 fitting metric

Fig. 12. Result from fitting parametric models in the least squares sense to the *alum-bronze* MERL BRDF. The scattering curves are shown for incident angles $\theta_i = 0°$ and $67°$. (a) shows the original Cook-Torrance model [Cook and Torrance 1982] fitted to the data using the E_2 error metric described in the text. In (b), the E_1 error metric is used. Figure (c) shows the E_2 fitting of the new microfacet model presented in this paper.

The proposed methods for importance sampling have been implemented in the PBRT stochastic path tracer [Pharr and Humphreys 2010] using BRDF importance sampling to generate ray directions, and multiple importance sampling for the last node in each path. The rendered scenes are shown in Figure 14. 14(a) shows a rendering using the original measured BRDF data, densely sampled at 40000 samples per pixel, and 14(b) shows the results from rendering using the BRDF models presented in this article with 1000 samples per pixel. 14(c) shows the same scene using the Ashikhmin-Shirley BRDF at 1000 samples per pixel. In the figures are insets with close-ups on geometry with a metallic paint, a type of BRDF with a high amount of wide-angle scattering. It shows the benefit of using a scatter distribution function which properly models off-specular scattering. Figure 15 shows a comparison of the developed importance sampling schemes to sampling using a hemispherical cosine PDF to weight samples.

In Figure 10, the C-parameter of the smooth surface BRDF model is shown for all measured BRDFs. For most BRDFs, C is between 0.5 and 1.5, and we have found the approximation $C = 1$, used for the PDF in the importance sampling scheme of the smooth surface model, to work well for the test cases. The leftmost bin, with $C < 0.25$, contains mostly fabric BRDFs, which have a scattering behaviour for which the new models are not designed.

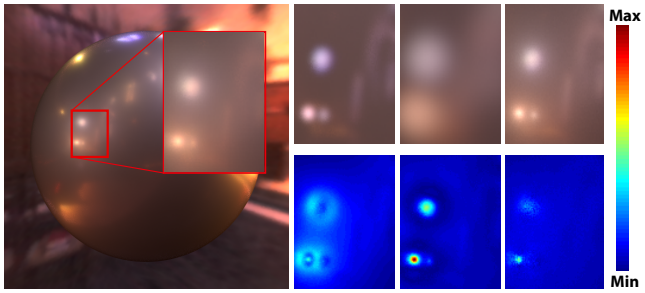

Fig. 13. Magnification of a sphere rendering using the *alum-bronze* BRDF. Figure (a) shows a rendering using the original measured data. Column (b) shows the Cook-Torrance model fitted to measured data using the E_1 error metric, and column (c) the Cook-Torrance model fitted to measured data using the E_2 error metric. Column (d) shows the new microfacet BRDF model fitted to data using the E_2 error metric. The upper images of (b)-(d) show the magnifications of the sphere rendered using the fitted models, while the bottom images show the colour-coded difference images with respect to the measured BRDF model.

To investigate energy conservation, the directional-hemispherical reflectance functions of three different BRDFs have been plotted in Figure 19. The two new models follow the directional-hemispherical reflectance of the measured BRDF until close to the grazing angle, where the apparent drop-off in the measured BRDF is not modelled. The smooth surface model does, however, conserve energy for the parameters resulting from fitting to measured data. The new microfacet model has an increase in reflectance near grazing, a common issue with microfacet shaders as shown in [Lewis 1993].

6. DISCUSSION

Two new BRDF models have been presented in this text, both showing the ability to give close fittings to measured scatter data for glossy surfaces. The micro-facet model has shown slightly lower fitting errors in most cases. It should be noted that data at grazing angles have been excluded from the fitting procedure, and that the calculations performed in this work indicate that the smooth surface model has better energy conservation properties at those angles. We believe the smooth surface BRDF is an important contribution, and that fitting results could be further improved by better approximation of the Fresnel factor.

The new models are more flexible in the types of surfaces which can be represented compared to the Cook-Torrance and Ashikhmin-Shirley models. This comes with the small additional cost of an extra parameter in the function determining the scatter distribution. When the scatter distribution is more Gaussian-like, one may therefore opt for one of the other models. A multi-lobe approach is also an alternative to increase fitting accuracy. This makes the optimization process of the data-fitting more demanding, however, with increasing cost and with local minima of the error metric becoming more of a problem [Ngan et al. 2005].

7. LIMITATIONS AND FUTURE WORK

The models presented are aimed at glossy surfaces. For BRDFs with other types of scattering behaviour, e.g. fabrics, our tests do not indicate improvements over previous models. Also, for nearly diffuse surfaces, small specular peaks occasionally appeared in the automatic fitting process. This may be explained by local minima of the error metric. The small peaks cause a small unwanted mirroring effect for the surfaces. With gloss being the focus of this article, we did not pursue better automatic fitting for these classes of BRDFs.

The choice of Fresnel factor is not optimal, as illustrated in the results section. We believe that many models, not only the models presented in this work, would benefit from better off-specular approximations to Fresnel reflectance and polarization effects. A thorough investigation of previous theoretical results, coupled with observation of experimental data, should be performed. The reflectance data employed in this work are unreliable close to the grazing angle, and we therefore also want to make measurements of different surfaces' grazing angle drop-off behaviour, to find other useful attenuation and obliquity factors.

A further investigation into different error metrics as well as their effect on the final rendered result would be valuable. For the new models, a visually better result was achieved when using a logarithmic error metric. This raises the interesting question of how to construct metrics for visually best results.

For the models presented in this paper, an empirical approach was taken, making design choices primarily based on observations of measured BRDF data. The observations are important for future work and modelling. The results, however, also indicate that theory not commonly used in computer graphics can be used for improving parametric modelling. Recent results in optical engineering, where accuracy is of high importance, could be interesting for computer graphics as well.

8. CONCLUSION

In this paper we have addressed the important area of accurate modelling of light-matter interaction for synthesis of realistic images, in particular surfaces exhibiting glossy scattering. In a study of measured BRDFs, we have observed the key properties which need to be modelled to yield an efficient and accurate representation of glossy scattering, in particular surfaces exhibiting sharp specular peaks and significant non-Lambertian wide-angle scattering. The observations also show consistencies with Rayleigh-Rice scattering theory for optically smooth surfaces. Based on the gained insights, and previous BRDF models used in computer graphics and optical engineering, two new BRDF models tailored for glossy surface scattering are presented. The parameters of the models affect the scattering distribution in a predictable way, which allows for artistic adjustment and control of appearance. The models lend themselves to efficient importance sampling for use in offline rendering.

ACKNOWLEDGMENTS

We would like to thank the anonymous reviewers for their constructive comments. We gratefully acknowledge Stefan Gustavson for invaluable discussions and feedback, and Matthew Cooper for proofreading the manuscript.

REFERENCES

ASHIKHMIN, M. AND SHIRLEY, P. 2000. An anisotropic phong brdf model. *Journal of Graphics Tools 5,* 2, 25–32.

BLINN, J. F. 1977. Models of light reflection for computer synthesized pictures. In *SIGGRAPH '77*. ACM, 192–198.

CHURCH, E. L. AND TAKACS, P. Z. 1991. The optimal estimation of finish parameters. In *Proceedings of SPIE*. Vol. 1530. 71–85.

CHURCH, E. L., TAKACS, P. Z., AND LEONARD, T. A. 1989. The prediction of brdfs from surface profile measurements. In *Proceedings of SPIE*. Vol. 1165. 136–150.

(a) Measured BRDF, 40000 samples/pixel

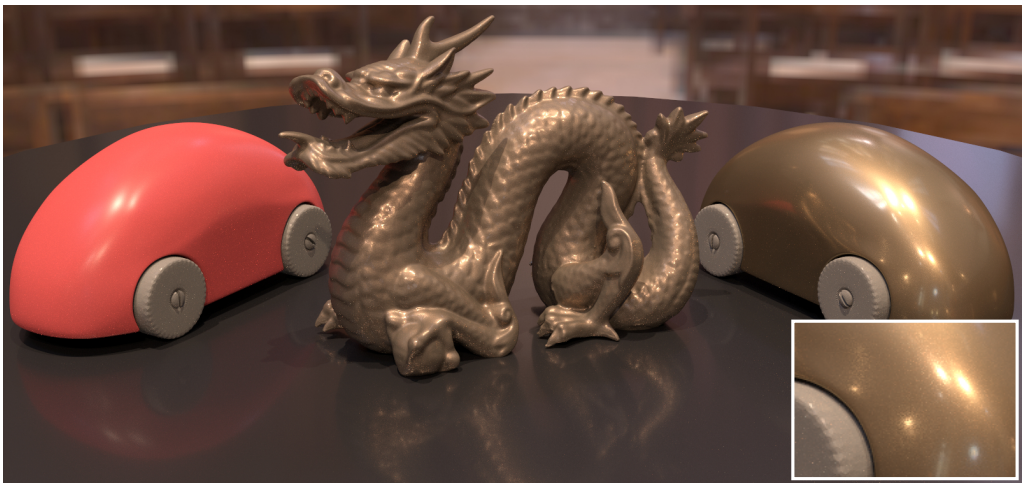

(b) New parametric BRDF models, 1000 samples/pixel

(c) Ashikhmin-Shirley, 1000 samples/pixel

Fig. 14. Renderings of an example scene using the PBRT Monte Carlo path tracer [Pharr and Humphreys 2010]. Figure (a) shows the scene using the original measured MERL BRDFs at 40000 samples/pixel. Figure (b) shows the scene using the new models presented in this article, rendered using importance sampling at 1000 samples/pixel. Figure (c) shows the same scene rendered using the Ashikhmin-Shirley model at 1000 samples/pixel. The insets at the lower right of the figures show a close-up on a highlight on the right car, to put focus on the wide-angle scattering reproduction of the different models. The geometries use the following BRDFs; table: *hematite*, left car: *purple-paint*, right car: *gold-metallic-paint3*, car wheels: *gray-plastic*, dragon: *alum-bronze*.

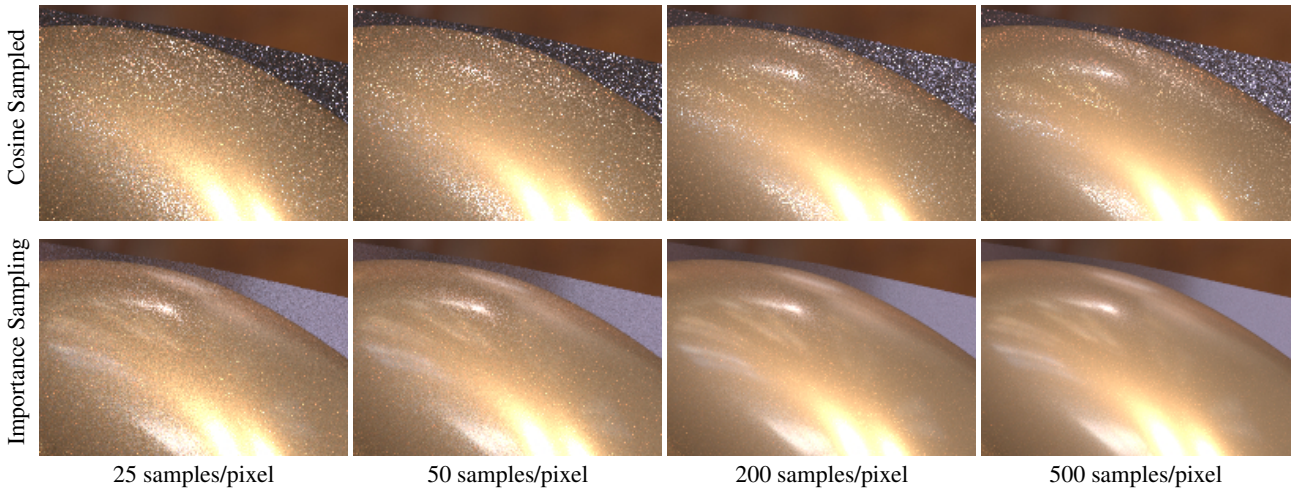

Fig. 15. A close-up from the example scene for a varying number of samples per pixel. The upper row shows renderings with varying number of samples/pixel for the new models using a hemispherical cosine PDF. The lower row shows renderings of the new models using the proposed importance sampling schemes.

COOK, R. L. AND TORRANCE, K. E. 1982. A reflectance model for computer graphics. *ACM Transactions on Graphics 1,* 1, 7–24.

EDWARDS, D., BOULOS, S., JOHNSON, J., SHIRLEY, P., ASHIKHMIN, M., STARK, M., AND WYMAN, C. 2006. The halfway vector disk for brdf modeling. *ACM Transactions on Graphics 25,* 1, 1–18.

HARVEY, J. E. 1977. Light scattering characteristics of optical surfaces. In *Proceedings of SPIE*. Vol. 107. 41–47.

HARVEY, J. E., KRYWONOS, A., AND STOVER, J. C. 2007. Unified scatter model for rough surfaces at large incident and scatter angles. In *Proceedings of SPIE*. Vol. 6672.

HE, X. D., TORRANCE, K. E., SILLION, F. X., AND GREENBERG, D. P. 1991. A comprehensive physical model for light reflection. *SIGGRAPH '91 25,* 4, 175–186.

KRYWONOS, A. AND HARVEY, J. E. 2006. Recent developments in the analysis of surface scatter phenomena. In *Proceedings of SPIE*. Vol. 6291.

LAFORTUNE, E. P. F., FOO, S.-C., TORRANCE, K. E., AND GREENBERG, D. P. 1997. Non-linear approximation of reflectance functions. In *SIGGRAPH '97*. ACM, 117–126.

LAWRENCE, J., BEN-ARTZI, A., DECORO, C., MATUSIK, W., PFISTER, H., RAMAMOORTHI, R., AND RUSINKIEWICZ, S. 2006. Inverse shade trees for non-parametric material representation and editing. *ACM Transactions on Graphics 25,* 3, 735–745.

LAWRENCE, J., RUSINKIEWICZ, S., AND RAMAMOORTHI, R. 2004. Efficient brdf importance sampling using a factored representation. In *ACM Transactions on Graphics (Proceedings of SIGGRAPH '04)*. ACM, 496–505.

LENSCH, H. P. A., GOESELE, M., CHUANG, Y.-Y., HAWKINS, T., MARSCHNER, S., MATUSIK, W., AND MUELLER, G. 2005. Realistic materials in computer graphics. In *SIGGRAPH '05: ACM SIGGRAPH 2005 Courses*. ACM, 1.

LEWIS, R. R. 1993. Making shaders more physically plausible. *Computer Graphics Forum 13,* 2, 109–120.

MATUSIK, W., PFISTER, H., BRAND, M., AND MCMILLAN, L. 2003. A data-driven reflectance model. *ACM Transactions on Graphics 22*, 759–769.

NEUMANN, L., NEUMANN, A., AND SZIRMAY-KALOS, L. 1999. Reflectance models with fast importance sampling. *Computer Graphics Forum 18*, 249–265.

NGAN, A., DURAND, F., AND MATUSIK, W. 2005. Experimental analysis of brdf models. In *Proceedings of the Eurographics Symposium on Rendering*. Eurographics Association, 117–226.

NICODEMUS, F. E., RICHMOND, J. C., HSIA, J. J., GINSBER, I. W., AND LIMPERIS, T. 1977. *Geometrical Considerations and Nomenclature for Reflectance*. U.S. Dept. of Commerce, National Bureau of Standards, NBS MN-160.

PHARR, M. AND HUMPHREYS, G. 2010. *Physically Based Rendering, Second Edition: From Theory To Implementation*. Morgan Kaufmann Publishers Inc.

RUMP, M., MÜLLER, G., SARLETTE, R., KOCH, D., AND KLEIN, R. 2008. Photo-realistic rendering of metallic car paint from image-based measurements. *Computer Graphics Forum 27,* 2 (Apr.), 527–536.

RUSINKIEWICZ, S. M. 1998. A new change of variables for efficient brdf representation. In *Eurographics Workshop on Rendering*. 11–22.

SCHLICK, C. 1994. An inexpensive brdf model for physically-based rendering. *Computer Graphics Forum 13*, 233–246.

STARK, M. M., ARVO, J., AND SMITS, B. 2005. Barycentric parameterizations for isotropic brdfs. *IEEE Transactions on Visualization and Computer Graphics 11,* 2, 126–138.

STOVER, J. C. 1995. *Optical Scattering: Measurement and Analysis, 2nd edition*. SPIE Publications.

TORRANCE, K. E. AND SPARROW, E. M. 1967. Theory for off-specular reflection from roughened surfaces. *Journal of the Optical Society of America 57,* 9, 1105–1112.

WALTER, B. 2005. Notes on the ward brdf. Tech. Rep. PCG-05-06, Cornell University.

WARD, G. J. 1992. Measuring and modeling anisotropic reflection. *SIGGRAPH '92 26,* 2, 265–272.

WESTIN, S. H., LI, H., AND TORRANCE., K. E. 2004. A field guide to brdf models. Tech. Rep. PCG-04-01, Cornell University.

WEYRICH, T., LAWRENCE, J., LENSCH, H., RUSINKIEWICZ, S., AND ZICKLER, T. 2008. Principles of appearance acquisition and representation. In *SIGGRAPH '08: ACM SIGGRAPH 2008 classes*. ACM, 1–119.

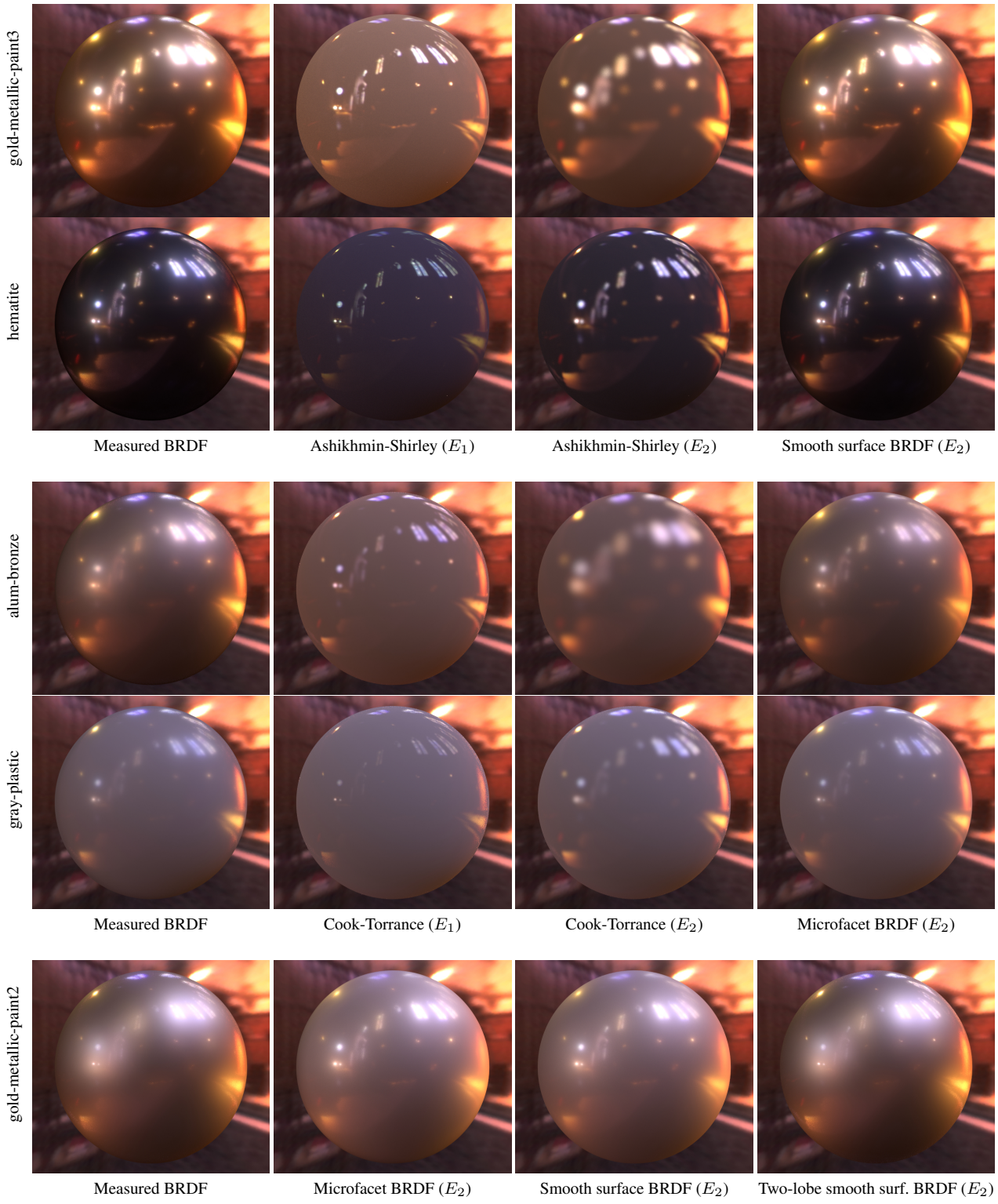

Fig. 16. Sphere renderings of five different BRDFs, *gold-metallic-paint3*, *hematite*, *alum-bronze*, *gray-plastic* and *gold-metallic-paint2*. The leftmost images show renderings using the original measured BRDF data. The rightmost images show renderings using the new BRDF models, fitted to data using the E_2 metric described in the text. For comparison, the Ashikhmin-Shirley and Cook-Torrance models, fitted to data using both of the E_1 and E_2 metrics, are shown in the middle. The bottom row shows the quality gain when using the two-lobe smooth surface model for *gold-metallic-paint2*, which has a distinct two-lobe shape (see Figure 3(b)).

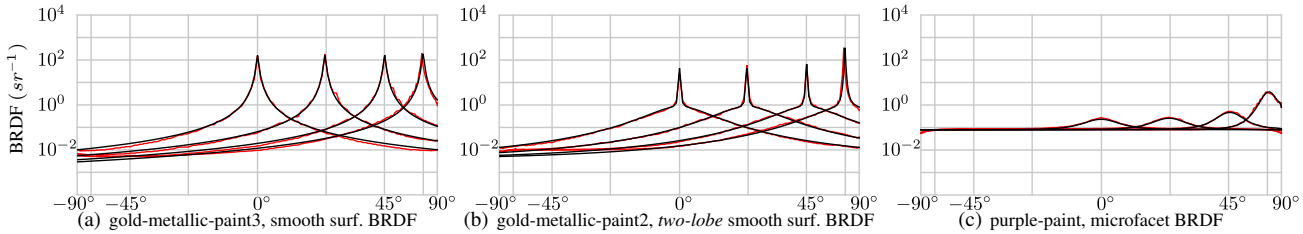

(a) gold-metallic-paint3, smooth surf. BRDF (b) gold-metallic-paint2, *two-lobe* smooth surf. BRDF (c) purple-paint, microfacet BRDF

Fig. 17. The presented BRDF models fitted to measured data. In the plots the scattering curve of the red colour channel is shown. The scattering curve of the parametric model is plotted in black and the original measured data in red.

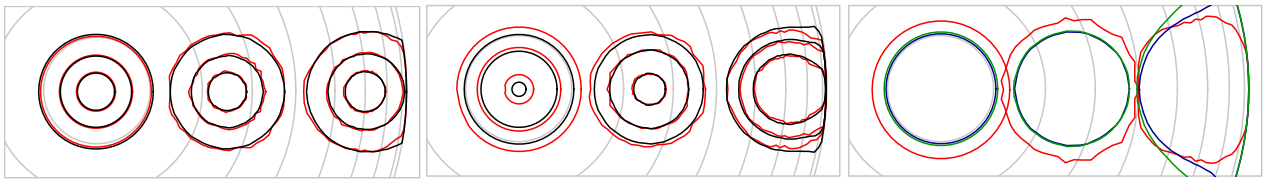

(a) gold-metallic-paint3, smooth surf. BRDF (b) purple-paint, microfacet BRDF (c) alum-bronze, microfacet BRDF in blue and smooth surf. BRDF in green

Fig. 18. BRDF models fitted to measured data. The plots show contour lines of the same levels for measured BRDF and fitted BRDF model. The plots in (a) and (b) show the high accuracy achieved by the presented models. A future challenge is to investigate and find more accurate approximations of attenuation and polarization effects to improve the fitting to scatter near grazing incident and outgoing angles for some BRDFs (c).

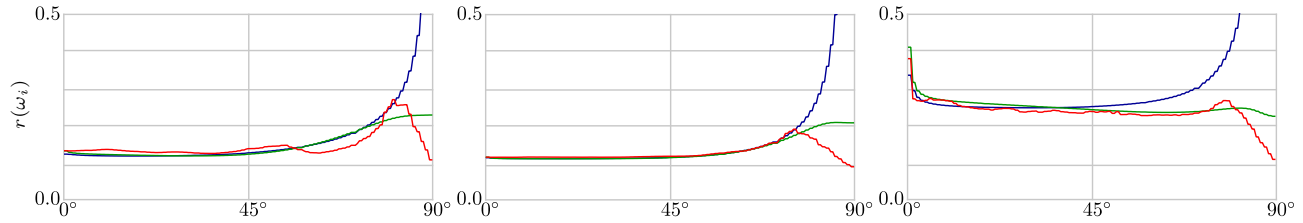

(a) alum-bronze (b) gray-plastic (c) gold-metallic-paint3

Fig. 19. Directional-hemispherical reflectance functions, $r(\omega_i)$, for the two new BRDF models fitted to the red channel of three different measured BRDFs. In red is the reflectance of the original measured data, in green is the reflectance of the smooth surface model and in blue the microfacet model. The models closely follows the directional-hemispherical reflectance of the measured BRDF, up to grazing incoming angle. The fitting procedure do not take this part of the original BRDF into consideration.

Table II. Square root of the fitting errors of BRDF models to selected measured BRDFs from the MERL database.

	Smooth surface BRDF $\sqrt{E_1(p)}$ / $\sqrt{E_2(p)}$	Microfacet BRDF $\sqrt{E_1(p)}$ / $\sqrt{E_2(p)}$	Cook-Torrance $\sqrt{E_1(p)}$ / $\sqrt{E_2(p)}$	Ashikhmin-Shirley $\sqrt{E_1(p)}$ / $\sqrt{E_2(p)}$
alum-bronze	0.2852 / 0.0765	0.2515 / 0.0638	0.3445 / 0.1112	0.3428 / 0.1103
gold-metallic-paint2	0.6412 / 0.1085	1.3965 / 0.1214	0.6792 / 0.1703	0.6802 / 0.1656
gold-metallic-paint3	1.1903 / 0.0384	2.0019 / 0.0451	2.2189 / 0.2033	2.2188 / 0.2031
gray-plastic	0.2353 / 0.0458	0.0957 / 0.0304	0.2076 / 0.0633	0.2075 / 0.0632
hematite	4.2070 / 0.0392	1.6654 / 0.0297	1.7595 / 0.1235	1.7595 / 0.1234
purple-paint	0.0507 / 0.0336	0.0313 / 0.0175	0.0411 / 0.0272	0.0455 / 0.0283